

On-chip quantum phonodynamics

Rusko Ruskov and Charles Tahan

Laboratory for Physical Sciences, 8050 Greenmead Dr., College Park, MD 20740*

Sound can be just as quantum as light. But our toolbox for single quanta of sound, i.e. phonons, is currently insufficient. Here we describe a new component that enables a chip-based, solid-state analogue of cavity-QED^{1,2} utilizing acoustic phonons instead of photons, phonitons instead of polaritons. We show how long-lived and tunable acceptor (hole) impurity states in silicon nanomechanical cavities can play the role of a matter non-linearity for coherent phonons just as, for example, the Josephson qubit plays in circuit-QED³. This system enables the control of single phonons and phonon-phonon interactions, dispersive phonon readout of the acceptor qubit, and compatibility with other nano/optomechanical components^{4,5} such as phonon-photon translators. Phonons, due to their unique properties, enable new opportunities for quantum devices and physics.

Circuit-QED has revolutionized the field of cavity-QED (cQED) providing a stable platform for light-matter interaction in the microwave regime along with large coupling strengths and solid state integrability. Progress in the field has enabled potential applications such as single microwave photon sources⁶ and quantum logic gates³ on a chip. In an ideal crystal environment, phonons may play a role analogous to photons, though they propagate with the much slower speed of sound. That acoustic phonons can be quantum coherent has been explored in a number of novel architectures, allowing seminal experiments in nanomechanical cooling^{4,7-9}, trapping of phonons in artificial phononic bandgap cavities^{5,9}, photon translation via phonons^{10,11}, and indirect qubit-phonon coupling^{12,13}. What is missing to complete the analogy for phonons is a non-linear element similar to an atom in cQED.

Such an element has been proposed recently¹⁴ where a single donor in silicon (P:Si or Li:Si) couples *directly* to confined phonons to form a hybrid state: a phoniton (direct analog of the polariton in cQED). The impurity-phonon interaction may be large due to large deformation potential matrix elements:¹⁵ $\langle \psi_s | \hat{D}_{ij} | \psi_s \rangle \sim \text{eV}$. The proposed system, however, requires very high frequencies (a few hundred GHz) and can be difficult to integrate with other phonon components. While other impurities such as in diamond¹³ or in III-V semiconductors are possible, a practical system in silicon would be highly desirable given recent demonstrations of high-Q cavities in silicon nanostructures⁹, silicon's investment in materials quality, and compatibility with CMOS technology and silicon photonics.

In this Letter we propose a new quantum circuit element based on a single acceptor (such as B, Al, In, etc.) embedded in a patterned silicon nano-membrane, that would be compatible with optomechanical components^{5,9}. The acceptor qubit, Fig. 1, is easily tunable in the range of 1 – 50GHz by external magnetic field, and also by additional electric field or strain. We show that the regime of strong resonant and also strong dispersive coupling of the qubit to a confined acoustic phonon is possible. We give explicit measurement protocols to observe the phonon vacuum Rabi splitting and readout of the phonon number state fine structure.

Engineering the qubit levels. Two acceptor qubit arrangements are possible based on the lifting of the 4-fold ground state degeneracy via external fields (see Methods). For a mag-

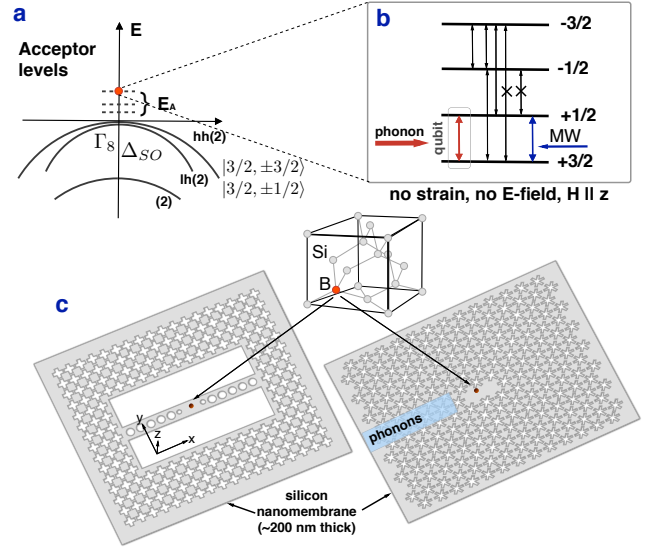


FIG. 1. (a) Hole valence bands in Si; 4-fold degeneracy at the band top (and of lowest acceptor states) corresponds to particles of spin $J = 3/2$ (Γ_8 representation of cubic symmetry, see, e.g. Ref.¹⁵). (b) Ground state splitting via external magnetic field along $[0, 0, 1]$ direction; allowed (forbidden) phonon transitions and qubit phonon driving (text). Level rearrangement is via additional strain. System manipulation via electric static/microwave fields is possible. (c) Examples of nanomechanical 1D and 2D phonon bandgap cavities reminiscent of already fabricated high-Q cavities in a patterned Si membrane^{5,9}. The acceptor is enclosed in the cavity and an on-chip phonon waveguide allows phonon coupling in/out of the system.

netic field $\mathbf{H}_z = (0, 0, H_z)$ along the crystal $[0, 0, 1]$ growth direction one can choose the lowest two Zeeman levels, $|\phi_1\rangle = |3/2\rangle$, $|\phi_2\rangle = |1/2\rangle$, as the qubit, which is the primary focus of this paper (Fig. 1b). The Zeeman type interaction is given by^{15,16}: $H_H = \mu_B \{g'_1 \mathbf{JH} + g'_2 (J_x^2 H_x + \text{c.p.})\}$; here c.p. is cyclic permutation of x, y, z ; J_x, \dots , etc. are the spin $3/2$ matrices (in the crystal directions), and the renormalized g -values g'_1, g'_2 (μ_B is Bohr magneton), depending on the acceptor bound states, fulfill the relations $|g'_1| \approx 1$, $|g'_2| \ll |g'_1|$ ^{15,17,18}. The qubit energy splitting $\delta E_H \simeq \mu_0 g'_1 H$ is tunable in the range $\approx 1 - 40$ GHz for $H = 0.1 - 3$ T. The cubic term in H_H lifts the level equidistance: the lowest and highest splitting

(Fig. 1b) are larger than the middle splitting by $\frac{3g'_2}{g'_1} \simeq 0.09$. For a field \mathbf{H} tilted away from the crystal axis $[0, 0, 1]$, the qubit splitting is weakly angle dependent.

Alternatively, a second qubit arrangement is possible with mechanical stress in addition to the magnetic field. Mechanical stress lifts the ground state degeneracy only partially: e.g., for stress along the crystal growth \hat{z} -direction (Fig. 1c), states $|\pm 3/2\rangle$ and $|\pm 1/2\rangle$ remain degenerate. Providing the stress causes an energy splitting larger than the splitting due to magnetic field \mathbf{H}_z , the level configuration in Fig. 1b rearranges so that the lowest (qubit) levels will be $|\phi'_1\rangle = |-1/2\rangle$, $|\phi'_2\rangle = |1/2\rangle$. This forms an alternate qubit, decoupled from phonons to first order; however, coupling can be switched on via electric field (see below). The effect of strain is described by the Bir-Pikus Hamiltonian¹⁵:

$$H_\varepsilon = d' \text{Tr} \varepsilon_{\alpha\beta} + b' \varepsilon_{xx} J_x^2 + \frac{d'}{\sqrt{3}} \varepsilon_{xy} \{J_x J_y\}_+ + \text{c.p.} \quad (1)$$

The renormalized deformation potential constants a', b', d' for acceptor B:Si can be estimated in the effective mass approximation (EMA)¹⁵, or extracted from experiment¹⁷; the latter gives $b' = -1.42 \pm 0.05 \text{ eV}$, $d' = -3.7 \pm 0.4 \text{ eV}$. Using H_ε , we estimate a splitting of $\delta E_\varepsilon \approx 1 - 10 \text{ GHz}$ for external stress in the range of $\sim 10^5 - 10^6 \text{ Pa}$. Such stress can be created in tensioned nanomechanical structures/membranes, improving also the mechanical Q -factor^{8,19}. A much larger stress ($\gtrsim 10^7 \text{ Pa}$) is possible due to a nearby (random) crystal defect²⁰ or for $[0, 0, 1]$ strain due to a SiGe substrate. The resulting splitting in the few hundred GHz range effectively suppresses the qubit-phonon coupling.

Strong coupling of acceptor to confined acoustic phonon. In order to calculate the qubit-phonon coupling (Methods) we consider a quantized phonon field in addition to any classical field. The coupling of the qubit $\{|3/2\rangle, |1/2\rangle\}$, is calculated to a plane wave mode $\varepsilon_{\text{vac}} \xi_{\mathbf{q}}^{(\sigma)} e^{-i\mathbf{q}\cdot\mathbf{r}}$ with polarization $\xi_{\mathbf{q}}^{(\sigma)}$ and energy $\hbar v_\sigma q$, that proved to be a good estimation of coupling to modes with realistic boundary conditions¹⁴ (Fig. 1c). The relevant matrix element is proportional to the ‘‘phonon vacuum field’’ strain, $\varepsilon_{\text{vac}} \equiv \left(\frac{\hbar}{2\rho\mathcal{V}v_\sigma q}\right)^{1/2}$ (ρ is the mass density, v_σ is sound velocity, and \mathcal{V} is the mode volume). For long-wave acoustic phonons, the coupling is (the acceptor is placed at maximum strain of the nanomechanical cavity):

$$g_\sigma^{3/2,1/2} = d' \left(\frac{\hbar\omega_{s's}}{8\rho\hbar^2\mathcal{V}v_\sigma^2}\right)^{1/2} \begin{cases} \cos\theta, \sigma = t_1 \\ i\cos 2\theta, \sigma = t_2 \\ -i\sin 2\theta, \sigma = l \end{cases} e^{-i\varphi}, \quad (2)$$

where the polar angles of the wave vector \mathbf{q} are with respect to \hat{z} -direction. Thus, the mode t_2 has a maximum along the phonon cavity ($\theta \approx \pi/2$), Fig. 1c. An alternative is to have an in-plane magnetic field \mathbf{H}_x along the crystal $[1, 0, 0]$ \hat{x} -direction (the latter is chosen to be along the phonon cavity): both modes t_1, t_2 (now at $\theta \approx 0$) are preferably coupled to the cavity. The maximal coupling $g_{\text{max},\sigma}^{3/2,1/2}$ scales as $\sqrt{\omega_{s's}/\mathcal{V}} \propto \sqrt{q/\mathcal{V}}$, as expected for a $(1s \rightarrow 1s)$ transition. Taking a cavity volume $\mathcal{V} \simeq d\lambda^2$ ($d = 200 \text{ nm}$ is the Si membrane thickness)

we get coupling in the range $g/2\pi \simeq 0.4 - 21 \text{ MHz}$ for the frequencies of $1 - 14 \text{ GHz}$ (Table 1). The other allowed transition $|3/2\rangle \rightarrow |-1/2\rangle$ (at twice the qubit frequency) is well detuned, while the transitions $|3/2\rangle \rightarrow |-3/2\rangle$, $|1/2\rangle \rightarrow |-1/2\rangle$ are phonon forbidden (Fig. 1b).

Generally, when the in-plane magnetic field has some angle θ_0 with the cavity (crystal x -axis), all transitions are allowed. Also, the qubit coupling to a preferably confined cavity phonon will change. As a qualitative example, consider a plane wave transverse mode t_1 (or t_2) along the x -axis ($\theta \approx 0$): the coupling will change in the same way as in Eq. (2), with θ replaced by θ_0 . This allows manipulation of the qubit-cavity coupling by rotation of the magnetic field.

Acceptor qubit relaxation rate. The qubit relaxation in the cavity is bounded by the bulk phonon emission rate $\Gamma_{\text{relax}} \lesssim \Gamma$, and reads:

$$\Gamma_{12}(\theta_0) = \frac{E_{12}^3}{20\pi\rho\hbar^4} \left\{ d'^2 (\cos^2 2\theta_0 + 1) \left[2/3v_l^5 + 1/v_l^5 \right] + b'^2 \sin^2 2\theta_0 \left[2/v_l^5 + 3/v_l^5 \right] \right\}; \quad (3)$$

here the contribution of longitudinal phonons is only a few percent (speeds of sound in Si: $v_l \simeq 1.7 \times v_t = 8.99 \times 10^3 \text{ m s}^{-1}$) and results in Table 1 are for $\theta_0 = 0$. Note that the coupling in this case can be switched off (e.g. for a t_1 -mode along \hat{x} -direction, at $\theta_0 = \pi/2$) while the relaxation cannot.

For the alternate qubit, $\{|-1/2\rangle, |1/2\rangle\}$, the stress and magnetic field are parallel along the growth \hat{z} -direction (Fig. 1c). Here both coupling and relaxation are zero in the absence of electric field and can be switched on using non-zero electric field \mathbf{E}_z in the same direction (Methods). It can be shown that the qubit-phonon coupling is given by the same Eq.(2) multiplied by a coupling factor, a function of the splitting ratios $r_h \equiv \frac{\delta E_H}{\delta E_\varepsilon}$, $r_e \equiv \frac{\delta E_E}{\delta E_\varepsilon}$: $f(r_h, r_e) = (\sqrt{z_+ z_-} - 1) / \sqrt{(1+z_+)(1+z_-)}$, with $z_\pm = (1 \pm \sqrt{(1 \mp r_h)^2 + r_e^2} \mp r_h)^2 / r_e^2$. Thus, e.g. for $r_h = 0.5 - 0.9$ this factor reaches $\approx 0.25 - 0.65$ for some optimal value of the electric field splitting, $r_e \lesssim 1$, which allows strong qubit-cavity coupling.

The relaxation time (Table 1) is comparable to T_1, T_2 measurements²³ in bulk Si at low B:Si doping ($8 \times 10^{12} \text{ cm}^{-3}$ or 500 nm acceptor spacing), where $T_{1,\text{exp}} \simeq 7.4 \mu\text{s}$ and $T_{2,\text{exp}}^* \simeq 2.6 \mu\text{s}$. While bulk T_2^* is limited by electric-dipole interacceptor coupling²⁴, both T_1, T_2 may improve for defect-free samples^{17,18}, isotopically purified Si²⁵, and single acceptors²⁰; T_1 may also improve in nanomembranes ($d \ll \lambda$) due to phase-space suppression. Finally, the relaxation to phonons is strongly suppressed since $(v_l/c)^3 \approx 10^{-15}$.

Phonon cavity loss. In the 1D/2D-phononic bandgap Si nanomembranes considered here (Fig. 1c), the main cavity loss mechanism is due to (fabrication) symmetry-breaking effects, coupling the cavity mode to unconfined modes, and also due to cavity surface defects²⁶. Bulk loss mechanisms are negligible in the GHz frequency range^{14,26}. The cavity Q -factor for frequencies of one to few tens GHz can be engineered in the range of $10^4 - 10^5$, or even higher^{9,26}.

Collecting all calculations in Table 1, one finds that *strong resonant coupling* is possible: $g_{12} \gg \Gamma_{12}, \kappa$ in a wide frequency range, allowing a number of Rabi flops, $\sim 30 - 100$.

parameter	symbol	circuit-QED	Quant Dot-QED	B:Si (1 GHz)	B:Si (4 GHz)	B:Si (8 GHz)	B:Si (1 Tesla)
resonance freq.	$\omega_r/2\pi$	5.7 GHz	325 THz	1 GHz	4 GHz	8 GHz	14 GHz
vac. Rabi freq.	$g/2\pi$	105 MHz	13.4 GHz	0.41 MHz	3.27 MHz	9.26 MHz	21.4 MHz
cavity lifetime	$1/\kappa, Q$	$0.64 \mu\text{s}, 10^4$	$5.5 \text{ ps}, 1.2 \cdot 10^4$	$15.9 \mu\text{s}, 10^5$	$4 \mu\text{s}$	$2 \mu\text{s}$	$1.14 \mu\text{s}$
qubit lifetime	$1/\Gamma$	84 ns	27 ps	$386.5 \mu\text{s}$	$6 \mu\text{s}$	$0.75 \mu\text{s}$	$0.14 \mu\text{s}$
critical atom #	$2\Gamma\kappa/g^2$	$\lesssim 8.6 \cdot 10^{-5}$	$\lesssim 1.87$	$\lesssim 4.9 \cdot 10^{-5}$	$\lesssim 2 \cdot 10^{-4}$	$\lesssim 3.9 \cdot 10^{-4}$	$\lesssim 6.9 \cdot 10^{-4}$
crit. phonon #	$\Gamma^2/2g^2$	$\lesssim 1.6 \cdot 10^{-4}$	$\lesssim 9.4 \cdot 10^{-2}$	$\lesssim 5.1 \cdot 10^{-7}$	$\lesssim 3.2 \cdot 10^{-5}$	$\lesssim 2.6 \cdot 10^{-4}$	$\lesssim 1.4 \cdot 10^{-3}$
# Rabi flops	$2g/(\kappa+\Gamma)$	~ 98	~ 0.8	~ 79	~ 99	~ 64	~ 34
cavity volume	\mathcal{V}	$10^{-6} \lambda^3$	-	$0.037 \lambda^3$	$0.148 \lambda^3$	$0.296 \lambda^3$	$0.52 \lambda^3$
wavelength	λ	5.26 cm	921 nm	5400 nm	1350 nm	675 nm	385 nm
dispersive coupling	$\chi \equiv g^2/\Delta$	17 MHz	-	0.04 MHz	0.33 MHz	0.93 MHz	2.14 MHz
peaks' resolution	$2\chi/\Gamma$	~ 6	-	~ 199	~ 25	~ 9	~ 4
# of peaks	$2\chi/\kappa$	~ 70	-	~ 8	~ 16	~ 23	~ 31

TABLE I. Key rates and parameters for circuit-QED²¹ (1D cavity), Quantum dot(QD)-QED²² (InAs QD embedded in a GaAs photonic crystal) vs. the B:Si phonon system in a patterned Si membrane (of thickness $d = 200 \text{ nm}$) phononic bandgap cavity; we show calculations for maximal coupling at frequencies of 1 GHz, 4 GHz, 8 GHz, and 14 GHz, for cavity volume $\mathcal{V} = d\lambda^2$ and $Q = 10^5$. The limiting frequency for strong dispersive coupling is reached at $\approx 21 \text{ GHz}$, when $\chi = \Gamma$. Number of Rabi flops, dispersive coupling, and dressed state's resolution parameters, $2\chi/\Gamma$, $2\chi/\kappa$, are comparable to that in circuit-QED and significantly surpass semiconductor quantum dots.

Here, a frequency of 1 GHz is the limit for $T \approx 20 \text{ mK}$ unless an active cavity cooling is performed⁹. Different energy scaling of the coupling and qubit relaxation sets a maximal energy splitting: $E_{12}^{\text{max}} = \frac{5}{4d} \sqrt{\frac{\rho \hbar^3 v_L^5}{\pi}} \approx 200 \text{ GHz}$. At such high frequencies the limiting factor would be the significant deterioration of the cavity Q -factor. Still, e.g., at 14 GHz even $Q = 10^3$ leads to strong coupling.

Observing the vacuum Rabi splitting. A suitable observable could be the averaged phonon cavity field amplitude $|\langle \hat{b} \rangle|$, which we have calculated, Fig. 2a-d, in the so-called ‘‘two-state approximation’’²⁷. On Fig. 2a we show the field amplitude spectrum for $\omega_a = \omega_r = 8 \text{ GHz}$ as two Rabi peaks at $\pm g$ vs. external phonon driving frequency ω_d , while Fig. 2c shows the ‘‘anticrossing picture’’ of the spectra at different acceptor-resonator detuning Δ_{ar} . Here the left resonance width and (normalized) height are $\Gamma_L = \sin^2 \Theta_0 \Gamma + \cos^2 \Theta_0 \kappa$ and $\cos \Theta_0$, respectively, while for the right resonance they are obtained via $\sin \Theta_0 \leftrightarrow \cos \Theta_0$, with $\tan(2\Theta_0) = 2g/\Delta_{\text{ar}}$.

Another experimental option to observe the dressed resonance(s) is to sweep the qubit detuning (via the \mathbf{H} -field) while keeping the probe input in resonance with the phonon cavity, Fig. 2d. As seen from Fig. 2c, the field amplitude will exhibit a resonant dip; it is shown for four different cavity frequencies, $\omega_r = 1, 4, 8, 14 \text{ GHz}$. For large detuning the resonance is approximately a Lorentzian (Fig. 2d) with a full width at half maximum, $\{\text{fwhm}\} \approx g^2/\kappa$ (a weak dependence on the qubit relaxation Γ is suppressed for strong couplings).

With increasing temperature the Rabi peak width will be broadened²⁸ by the factor $1 + 2n_{\text{th}}$ and the peak height will decrease by $2p_{\text{st}} - 1$, where $p_{\text{st}} = (1 + n_{\text{th}})/(1 + 2n_{\text{th}})$ is the ground state occupation number. These expressions are applicable at low temperatures, when the average thermal phonon number $n_{\text{th}} \equiv 1/(\exp[\hbar\omega_r/k_B T] - 1)$ is small ($n_{\text{th}} \lesssim 0.2$ see, e.g., Ref.²⁹). For $\omega_r/2\pi = 8 \text{ GHz}$ the Rabi peaks will be seen at 350 mK, but are negligible at 1 K (Fig. 2b). Actually, at higher temperatures, when $n_{\text{th}} \gtrsim 1$, the lowest dressed states become saturated and in addition to these there will appear two broadened peaks (inside the Rabi doublet, Fig. 2a), roughly at frequencies $\pm g[\sqrt{n+1} - \sqrt{n}]$, $n \approx n_{\text{th}}$, so that at 1 K

these peaks will dominate over the Rabi peaks²⁹. These peaks could be a first quantum signature of acceptor-resonator coupling, when experiments are performed at the relatively high temperature of 1 K.

Measurement via photons and standard techniques. The phonon probing can be performed using a recently proposed phonon-to-photon translator (PPT)³⁰ that can be realized on the same patterned Si nanomembrane with a simultaneous photon/phonon bandgap structure, Fig. 1c. The translator allows for optical measurement techniques to be applied to phononic components. We show in Fig. 2e a schematic of the experiment, designed to measure the phonon cavity field amplitude $\langle \hat{b} \rangle$ via a heterodyne optical measurement²⁸. To be able to scan around the mechanical resonance ω_r , one needs optical frequency resolution (at $\omega/2\pi \approx 200 \text{ THz}$ ³⁰) better than the dressed state peak width, $(\Gamma + \kappa)/2\pi \approx 30 - 150 \text{ kHz}$, (at $\omega_r/2\pi \approx 4 - 8 \text{ GHz}$, Table 1). This can be achieved by stabilization of the external photon probe to a bandwidth of tens of kHz. In the on-chip implementation of the PPT interface no photon should be allowed to enter the phonon system, to avoid ionization of the acceptor (Methods). However, the estimated ionization cross section is small, $\sigma_{\text{phot}} \approx 8.6 \times 10^{-23} \text{ m}^2$, since interband transitions are forbidden: $\hbar\omega \approx 0.82 \text{ eV} < \text{indirect bandgap in Si}$, and due to the final state energy suppression, $\sim 1/E_f^{3.5}$. (For 10 photons in the cavity volume $d\lambda^2$ one gets an acceptor lifetime of $12 \mu\text{s}$, assuming maximum photon-acceptor overlap.) Note that ionization can be further suppressed in regions of low photon intensity.

The strong *dispersive coupling* regime is also reachable. The dispersive coupling, $\chi \equiv g^2/\Delta_{\text{ar}}$, ranges from 0.04 MHz to 2.14 MHz for the frequencies presented (Table 1). Since the conditions $\Delta_{\text{ar}} \geq 10g$ (dispersive regime) and $g^2/\Delta_{\text{ar}}\Gamma_{\text{relax}} \geq 1$ (good resolution of phonon number peaks) can be well fulfilled in the GHz range, this would allow an experiment on resolving the number states in the phononic cavity. In the dispersive regime one can apply two tones (as in circuit-QED²¹): here, one tone is a *phonon* probe at ω_d , slightly detuned from the resonator frequency ω_r (Fig. 2e). The second (spectro-

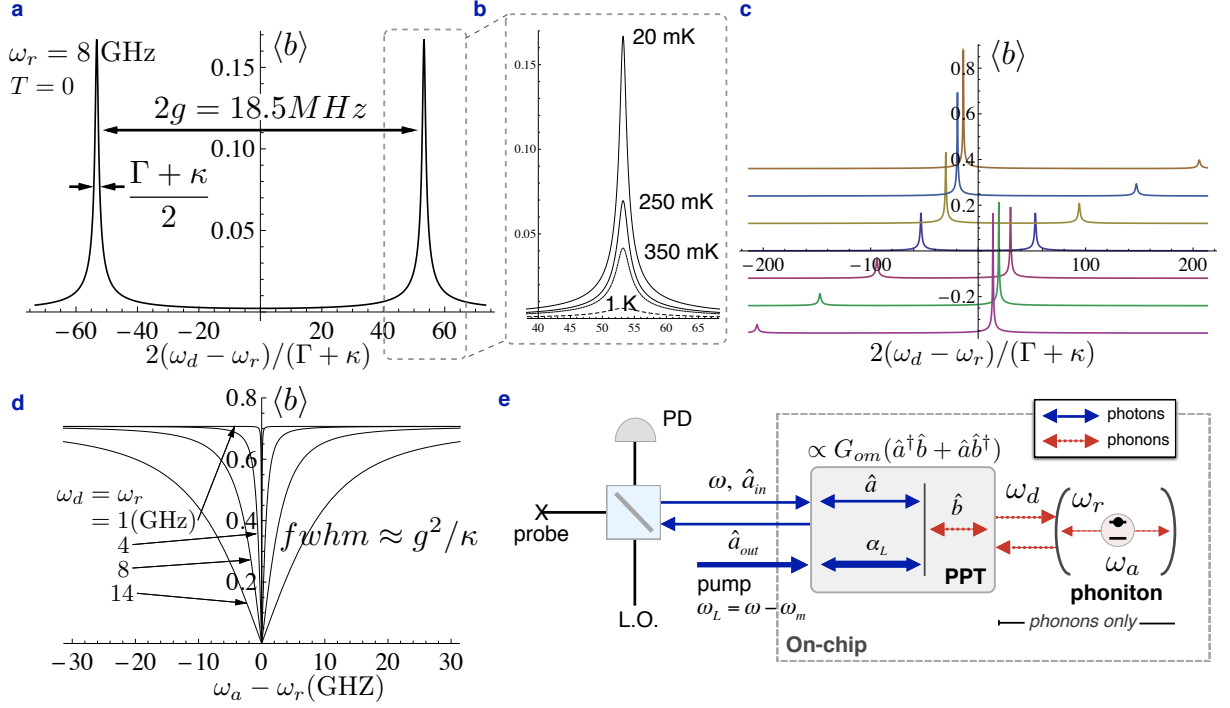


FIG. 2. Experimental signatures of a phonon system. (a) Rabi splitting in the strong resonant coupling regime as a function of a phonon probe signal sweep. (b) Rabi peaks vs. temperature (approximate). At $n_{th} \gtrsim 1$ broad peaks will appear inside the Rabi doublet (not shown) due to transitions to higher dressed states (see text). (c) “Anticrossing picture” at qubit-phonon cavity detuning; for large positive detuning (upmost curve), the left resonance is dispersively shifted by $-g^2/\Delta_{ar}$ while the other (detuned) resonance is strongly suppressed as $\sin\Theta_0$ (see text). (d) An alternative experiment to determine the Rabi splitting: the absorption spectrum as a function of qubit detuning (via a magnetic field sweep). (e) Schematics of the standard optical heterodyne reflection experiment of the phonon system utilizing a high-efficiency coherent photon-to-phonon translator.

scopic) tone, at ω_{sp} , is driving some of the dressed transitions around the acceptor frequency ω_a via direct microwave (MW) electric driving, that is similar to a MW manipulation of individual nitrogen-vacancy centers¹³ (for B:Si a stronger coupling to electric MWs is expected compared to NVs since the acceptor dipole coupling is $p_E \simeq 30\mu_B/c^{18,23}$). Thus, one could measure the reflection by the phononic bandgap resonator of the first (phononic) tone as a function of the MW spectroscopic tone ω_{sp} , and eventually observe the fine spectral structure of the dressed cavity-acceptor system³¹. We note that other measurement approaches are possible via, e.g., hole transport^{20,32}, STM probe spectroscopy³³, or direct single-phonon detection³⁴.

Discussion and applications. We have introduced a system that allows for on-chip manipulation of coherent acoustic phonons via coupling to acceptor qubit states in a nanomechanical cavity. Hybridization of the phonon-acceptor system and strong dispersive coupling are both possible with comparable parameters to circuit-QED²¹ and far surpassing semiconductor quantum dot QED²². The phonon component can be incorporated in more complex systems such as with phonon-photon interfaces to photonics^{9,30}, and in arrays of other phonon systems for engineered many-body phonon devices^{14,35}. From the perspective of qubits, the isolated acceptor provides a potentially robust two-level system for quan-

tum information processing. The phonon component described here offers an avenue for phonon dispersive readout of acceptor qubit states and the potential for spin qubit-to-photon conversion in silicon - which would be a seminal accomplishment.

I. METHODS

Origin of strong acceptor-phonon coupling. The role of an atom can be taken by a single impurity in a host crystal, e.g. in Si¹⁴. The impurity-acoustic phonon interaction¹⁵, $H_{e,ph}^{ac}(\mathbf{r}) = \sum_{ij} \hat{D}_{ij} \hat{\epsilon}_{ij}(\mathbf{r})$, may lead to a strong coupling regime ($g > \Gamma_{relax}, \kappa$) even for cavity effective volume of few tens¹⁴ of $\sim \lambda^3$, since the deformation potential matrix elements are large:¹⁵ $\langle \psi_s | \hat{D}_{ij} | \psi_s \rangle \sim eV$. Qualitatively, the large coupling can be traced from the much smaller bandgap ($\sim eV$) in the “Si-vacuum” as compared to QED ($\sim 10^6 eV$).

Hole valence bands in Si. Holes in Si require a richer physical picture^{15,16} (compared to positrons in QED). The 4-fold degeneracy (Fig. 1a) at the top of the valence band (neglecting heavy-light hole splitting) corresponds to propagation of particles of spin $J = 3/2$, reflecting the Γ_8 representation of cubic symmetry. Relatively large spin-orbit coupling implies a 2-fold degenerate band (Γ_7 representation), split-off by an

energy gap $\Delta_{SO} \simeq 45 \text{ meV}^{15}$. For shallow acceptor centers in Si (e.g., B, Al, In, etc) the ionization energy, $E_A \sim \Delta_{SO}$: thus, all valence bands will play a role in the acceptor states. Still, the lowest acceptor states remain 4-fold degenerate since the acceptor spherical (Coulomb) potential does not change the cubic symmetry of the host crystal¹⁵.

Engineering the qubit levels. The role of electric field. The degeneracy of the ground state can be lifted by external magnetic field via the Zeeman type interaction H_H (Fig. 1b), and via mechanical strain, Eq.(1). The related Hamiltonians are invariants of the cubic symmetry group $O_h = T_d \times I$ and time reversal^{15,16} and are constructed from the momentum operator, $k_\alpha = \frac{1}{i} \frac{\partial}{\partial x_\alpha} + \frac{e}{c} A_\alpha$ (or the corresponding fields¹⁵) and the spin-3/2 operators J_α , $\alpha = x, y, z$.

For a relatively weak electric field \mathbf{E} the linear Stark effect is possible:

$$H_E = \frac{PE}{\sqrt{3}} (E_x \{J_y J_z\}_+ + E_y \{J_z J_x\}_+ + E_z \{J_x J_y\}_+), \quad (4)$$

since an ion impurity actually reduces the cubic symmetry ($T_d \times I$) to T_d (and thus, there is no invariance under inversion)¹⁵. The ground state splits to two doubly degenerate levels; however, the H_E does not commute with J_z for any direction of the field \mathbf{E} , leading to mixing of the Zeeman states. The latter can be useful to switch on/off the phonon coupling of the alternate qubit, $\{|-1/2\rangle, |1/2\rangle\}$, provided the splitting $\delta E_E = 2p_E |\mathbf{E}|$ is of the order of that due to stress, e.g., in the GHz range. The transition electric dipole moment, p_E , can be extracted from experiments: bulk dielectric absorption measurements¹⁸ give $p_E \simeq 0.26D$, with $D = 3.336 \times 10^{-30} \text{ C m}$ being the Debye unit for e.d.m. (this is supported by single acceptor transport experiments²⁰). Thus, a splitting of 1 GHz requires an electric field $|\mathbf{E}|_{1\text{GHz}} \simeq 3.85 \times 10^5 \text{ V/m}$, achievable in nanodevices³². Note, however, that increasing the field (splitting) exponentially decreases the qubit life time due to acceptor ionization: for $\delta E = 1 \text{ GHz}$ the life time is $\tau_{\text{ion}} \approx 12 \text{ s}$, while for $\simeq 1.26 \text{ GHz}$ it is $\tau_{\text{ion}} \approx 12 \text{ ms}$, etc³².

These numbers show that there is an experimental ‘‘window’’ for the alternate qubit, $\{|-1/2\rangle, |1/2\rangle\}$, introduced in the main text. For example, for a qubit (Zeeman) splitting of $\delta E_H = 1 \text{ GHz}$ and a strain splitting $\delta E_e = 1.43 \text{ GHz}$ (ratio of $r_h \equiv \frac{\delta E_H}{\delta E_e} = 0.7$) the coupling factor reaches the maximal value of $f(r_h, r_e) \simeq 0.4$ for $\delta E_E = 1 \text{ GHz}$, i.e., $r_h = 0.7$. Analogously, for a qubit splitting of $\delta E_H = 2 \text{ GHz}$ this electric field splitting leads to the same coupling factor of 0.4, giving a possibility for a strong acceptor-phonon coupling, Eq.(2), and a relatively long (static field) ionization life time.

Strong coupling of acceptor to confined acoustic phonon. We account for the acceptor coupling to a quantized phonon field starting from the Bir-Pikus Hamiltonian, derived for a uniform classical strain field, Eq.(1). For low-energy acoustic phonons the interaction Hamiltonian, \hat{H}_{ph} , has the form of Eq.(1), with the strain operator $\hat{\epsilon}_{ij}(\mathbf{r}) = \frac{1}{2} \left(\frac{\partial u_i}{\partial r_j} + \frac{\partial u_j}{\partial r_i} \right)$ expressed via the quantized mechanical displacement: $\mathbf{u}(\mathbf{r}) = \sum_{\mathbf{q}\sigma} \left(\mathbf{u}_{\mathbf{q}\sigma}(\mathbf{r}) b_{\mathbf{q}\sigma} + \mathbf{u}_{\mathbf{q}\sigma}^*(\mathbf{r}) b_{\mathbf{q}\sigma}^\dagger \right)$. The mode normalization is $\int d^3 \mathbf{r} \mathbf{u}_{\mathbf{q}\sigma}^*(\mathbf{r}) \mathbf{u}_{\mathbf{q}\sigma}(\mathbf{r}) = \frac{\hbar}{2\rho\omega_{\mathbf{q}\sigma}}$, so that $b_{\mathbf{q}\sigma}^\dagger$ creates a phonon in

the mode (\mathbf{q}, σ) with energy $\hbar\omega_{\mathbf{q}\sigma}$ (ρ is the material mass density) in a mode volume \mathcal{V} . The vector \mathbf{q} denotes a collective index of the discrete phonon mode defined via the phonon cavity boundary conditions and mode volume \mathcal{V} . Similar to cavity QED²⁸, the phonon-acceptor coupling $\hbar g_{\mathbf{q}\sigma}^{s's} \equiv \langle s'; \mathbf{q}\sigma | H_{\text{ph}} | s \rangle$ enters in a Jaynes-Cummings Hamiltonian (see, e.g. Ref.¹⁴): $H_g \approx \hbar g_{\mathbf{q}\sigma}^{s's} \left(\sigma_{s's}^+ b_{\mathbf{q}\sigma} + \sigma_{s's}^- b_{\mathbf{q}\sigma}^\dagger \right)$, where we only retain the resonant cavity phonon, and $\sigma_{s's}^\pm \equiv |s'\rangle \langle s|$ refers to the relevant acceptor transition.

Phonon-photon translator. Such a device is based on optomechanical non-linearities that couple in the same bandgap cavity (see Fig. 2e) two photon modes (\hat{a}, \hat{a}_p) and a phonon mode \hat{b} , via optomechanical coupling h_{om} ³⁰. For photons in the near-infrared range ($\lambda_{opt} \approx 1500 \text{ nm}$) the PPT allows one to couple a quantum optical input/output channel (of frequency $\omega/2\pi \simeq 200 \text{ THz}$) to a phonon channel (with $\omega_d/2\pi \simeq 4 - 8 \text{ GHz}$), and the coupling between the fields is enhanced by the auxiliary photon pump channel, pumping at the sideband resolved frequency $\omega_p = \omega - \omega_m - \Delta$ (at pump detuning $\Delta = 0$ it is at resonance with the red sideband of mode ω). The coherent nature of the photon-to-phonon translator is described by the effective beam-splitter type Hamiltonian³⁶:

$$H_{b-s} = -\Delta \hat{b}^\dagger \hat{b} + G_{om} \left(\hat{a}^\dagger \hat{b} + \hat{a} \hat{b}^\dagger \right) \quad (5)$$

where $G_{om} \propto h_{om} E_0$ is the enhanced effective coupling, proportional to the pump field amplitude, E_0 . The weak coupling regime, $G_{om} < \kappa^{opt}$ is needed to avoid total optical reflection, and optimal translation (close to 100%) takes place at a matching condition³⁰ $G_{om} = \sqrt{\kappa^{mech} \kappa^{opt}}$ (κ^{mech} , κ^{opt} are the couplings of the PPT to respective waveguides).

Acceptor ionization via optical photons. Since the photon-to-phonon translator is realized on the same Si nanomembrane (implying a simultaneous photonic/phononic bandgap structure) it is natural to ask how 200 THz photons may affect the qubit lifetime when they reach the acceptor. The corresponding photon energy of 0.82 eV is less than the indirect bandgap in Si ($\Delta E_{\text{gap}} = 1.1 \text{ eV}$) and thus interband transitions are not possible. Thus, one considers an ‘‘ionization process’’ of a bound hole going to the continuous spectrum, an analog of the ionization of an (anti)hydrogen atom (the corresponding cross section is thus re-scaled). Correspondingly, one uses the re-scaled values: a free hole mass $m_A \simeq 0.23 m_e$ in Si, an effective Bohr radius $a_A^{\text{eff}} = \frac{e^2 Z}{2[4\pi\epsilon_0\epsilon_r]E_A}$, with the acceptor ionization energy for B:Si, $E_A \approx 0.044 \text{ eV}$, and screening factor $Z \simeq 1.4$. The total cross section is:

$$\sigma_{\text{phot}} = \frac{32\pi}{3} \frac{\hbar^6}{c\sqrt{2m_A m_A^3} [a_A^{\text{eff}}]^5 E_f^{2.5} (E_f + E_A)} \frac{1}{[4\pi\epsilon_0\epsilon_r]}, \quad (6)$$

where $E_f = \hbar\omega - E_A$ is the final (free) hole energy, and $c = c_0/\sqrt{\epsilon_r}$ is the speed of light in Si ($\epsilon_r^{\text{Si}} \simeq 11.9$). Since $E_A \ll E_f$, the total cross section is suppressed as $\propto 1/E_f^{3.5}$. Given n_c photons in cavity volume \mathcal{V} the acceptor life time is $\tau_{\text{phot}} = 2\mathcal{V}/(n_c c \sigma_{\text{phot}})$ for a maximum photon-acceptor overlap.

- * charlie@tahan.com, ruskovr@gmail.com
- ¹ Kimble, H. J. Strong interactions of single atoms and photons in cavity QED. *Physica Scripta* **T76**, 127–137 (1998).
 - ² Raimond, J. M., Brune, M. & Haroche, S. Colloquium: Manipulating quantum entanglement with atoms and photons in a cavity. *Rev Mod Phys* **73**, 565–582 (2001).
 - ³ Blais, A., Huang, R. S., Wallraff, A., Girvin, S. M. & Schoelkopf, R. J. Cavity quantum electrodynamics for superconducting electrical circuits: An architecture for quantum computation. *Phys. Rev. A* **69**, 62320 (2004).
 - ⁴ Kippenberg, T. J. & Vahala, K. J. Cavity optomechanics: Back-action at the mesoscale. *Science* **321**, 1172–1176 (2008).
 - ⁵ Eichenfield, M., Chan, J., Camacho, R. M., Vahala, K. J. & Painter, O. Optomechanical crystals. *Nature* **462**, 78–82 (2009).
 - ⁶ Houck, A. A. *et al.* Generating single microwave photons in a circuit. *Nature* **449**, 328–331 (2007).
 - ⁷ Rocheleau, T. *et al.* Preparation and detection of a mechanical resonator near the ground state of motion. *Nature (London)* **463**, 72 (2010).
 - ⁸ Teufel, J. D. *et al.* Sideband cooling of micromechanical motion to the quantum ground state. *Nature (London)* **475**, 359–363 (2011).
 - ⁹ Chan, J. *et al.* Laser cooling of a nanomechanical oscillator into its quantum ground state. *Nature* **478**, 89–92 (2011).
 - ¹⁰ Dong, C., Fiore, V., Kuzyk, M. C., Tian, L. & Wang, H. Optical wavelength conversion via optomechanical coupling in a silica resonator. *arXiv* 1205.2360v1.
 - ¹¹ Hill, J. T., Safavi-Naeini, A. H., Chan, J. & Painter, O. Coherent optical wavelength conversion via cavity-optomechanics. *arXiv* 1206.0704v1.
 - ¹² O’Connell, A. D. *et al.* Quantum ground state and single-phonon control of a mechanical resonator. *Nature* **464**, 697 (2010).
 - ¹³ Kolkowitz, S. *et al.* Coherent sensing of a mechanical resonator with a single-spin qubit. *Science* **335**, 1603–1606 (2012).
 - ¹⁴ Soykal, Ö. O., Ruskov, R. & Tahan, C. Sound-based analogue of cavity quantum electrodynamics in silicon. *Phys. Rev. Lett.* **107**, 235502 (2011).
 - ¹⁵ Bir, G. L. & Pikus, G. E. *Symmetry and Strain-induced Effects in Semiconductors* (Keter Publishing House, Jerusalem, 1974).
 - ¹⁶ Luttinger, J. M. Quantum theory of cyclotron resonance in semiconductors: General theory. *Phys. Rev.* **102**, 1030–1041 (1956).
 - ¹⁷ Neubrand, H. ESR from boron in silicon at zero and small external stress: I. line positions and line structure. *Phys. Stat. Solidi (B)* **86**, 269–275 (1978).
 - ¹⁸ Köpf, A. & Lassmann, K. Linear Stark and nonlinear Zeeman coupling to the ground state of effective mass acceptors in silicon. *Phys. Rev. Lett.* **69**, 1580–1583 (1992).
 - ¹⁹ Verbridge, S. S., Shapiro, D. F., Craighead, H. G. & Parpia, J. M. Macroscopic tuning of nanomechanics: Substrate bending for reversible control of frequency and quality factor of nanostring resonators. *Nano Letters* **7**, 1728–1735 (2007).
 - ²⁰ Calvet, L. E., Wheeler, R. G. & Reed, M. A. Observation of the linear stark effect in a single acceptor in Si. *Phys. Rev. Lett.* **98**, 096805 (2007).
 - ²¹ Schuster, D. I. *et al.* Resolving photon number states in a superconducting circuit. *Nature* **445**, 515–518 (2007).
 - ²² Bose, R., Sridharan, D., Kim, H., Solomon, G. S. & Waks, E. Low-photon-number optical switching with a single quantum dot coupled to a photonic crystal cavity. *Phys. Rev. Lett.* **108**, 227402 (2012).
 - ²³ Song, Y. P. & Golding, B. Manipulation and decoherence of acceptor states in silicon. *EPL* **95**, 47004 (2011).
 - ²⁴ Golding, B. & Dykman, M. I. Acceptor-based silicon quantum computing. *arXiv* cond-mat/0309147v1.
 - ²⁵ Karaiskaj, D., Kirczenow, G., Thewalt, M. L. W., Buczko, R. & Cardona, M. Origin of the residual acceptor ground-state splitting in silicon. *Phys. Rev. Lett.* **90**, 016404 (2003).
 - ²⁶ Chan, J., Safavi-Naeini, A. H., Hill, J., Meenehan, S. & Painter, O. Optimized optomechanical crystal cavity with acoustic radiation shield. *arXiv* 1206.2099v1.
 - ²⁷ Tian, L. & Carmichael, H. J. Quantum trajectory simulations of the two-state behavior of an optical cavity containing one atom. *Phys. Rev. B* **46**, R6801–R6804 (1992).
 - ²⁸ Walls, D. F. & Milburn, G. J. *Quantum Optics* (Springer, Berlin 2008, 2008).
 - ²⁹ Fink, J. M. *et al.* Quantum-to-classical transition in cavity quantum electrodynamics. *Phys. Rev. Lett.* **105**, 163601 (2010).
 - ³⁰ Safavi-Naeini, A. H. & Painter, O. Proposal for an optomechanical traveling wave phonon-photon translator. *New Journal of Physics* **13**, 013017 (2011).
 - ³¹ Dykman, M. I. & Krivoglaz, M. A. Profiles of no-phonon lines of impurity centers interacting with local or quasiloc vibrations. *Sov. Phys. Solid State* **29**, 210–214 (1987).
 - ³² Smit, G. D. J., Rogge, S., Caro, J. & Klapwijk, T. M. Stark effect in shallow impurities in Si. *Phys. Rev. B* **70**, 035206 (2004).
 - ³³ Fuechsle, M. *et al.* Spectroscopy of few-electron single-crystal silicon quantum dots. *Nature Nanotechnology* **5**, 502–505 (2010).
 - ³⁴ Gustafsson, M. V., Santos, P. V., Johansson, G. & Delsing, P. Local probing of propagating acoustic waves in a gigahertz echo chamber. *Nature Physics* **8**, 338–343 (2012).
 - ³⁵ Rabl, P. *et al.* A quantum spin transducer based on nano-electromechanical resonator arrays. *Nature Physics* **6**, 602–608 (2010).
 - ³⁶ Zhang, J., Peng, K. & Braunstein, S. L. Quantum-state transfer from light to macroscopic oscillators. *Phys. Rev. A* **68**, 013808 (2003).